RSC Advances

PAPER

View Article Online
View Journal | View Issue

Cite this: *RSC Adv.*, 2025, **15**, 35265

Synthesis and characterization of thermolatent bases with varying activation temperatures

Matthias Udo Mayer-Kriehuber,[ab] Evelyn Sattler,[a] David Reisinger,[ab] Daniel Bautista-Anguís,[ab] Szymon Gaca,[ab] Christoph Schmidleitner,[ac] Ivica Duretek,[b] Elvira Vidovic[d] and Sandra Schlögl[ab]

Latent catalysts offer a powerful means to control both the start and progress of polymerization reactions by releasing the active species only upon exposure to a defined external stimulus, such as heat or light. While their application is well-established in coatings and adhesives, the concept is gaining traction for spatiotemporally controlling bond exchange reactions in dynamic polymer networks, particularly for balancing creep and flow properties. Latent catalysis does not only enable targeted property control in dynamic polymer networks, but also supports circular polymer strategies by allowing repair, reshaping, and recycling without loss of performance. These capabilities can extend the materials' lifetime, reduce the need for energy-intensive virgin polymer production, and contribute to lowering the carbon footprint of polymer manufacturing. In this study, we report on the synthesis and thermal characterization of a library of thermolatent Brønsted base generators (TBGs), designed to release catalytically active bases upon thermal activation. These TBGs consist of strong organic bases ionically bonded to carboxylate anions derived from acetic acid derivatives and dicarboxylic acids with varying chain length, which act both as stabilizing counterions and as thermally labile groups. This work systematically explores the relationship between molecular structure and thermal stability of TBGs, with particular focus on how structural variations in carboxylate anions and base cations influence the activation temperature. The synthesized compounds are highly stable under ambient conditions and decompose over a broad temperature range (60 °C to 290 °C), depending on the chemical structure of the acid as well as the base. The cleavage events observed during thermal activation results in an efficient and irreversible release of the base.

Received 16th July 2025
Accepted 18th September 2025

DOI: 10.1039/d5ra05095b

rsc.li/rsc-advances

1 Introduction

The use of latent catalysts is a well-established strategy to ensure an extended shelf life of one-pot curing systems. Whilst they have only slight – or in some cases no – reactivity under storage conditions, they efficiently initiate the curing/polymerization reaction as soon as an appropriate external trigger is applied. Among the various external stimuli, temperature and light are the most commonly applied ones, due to lower costs and operational safety.[1,2]

The photo-induced release of Brønsted acids and bases provides a convenient way to cure coatings, adhesives or photoresists under ambient conditions and in a spatially controlled manner.[3] In particular, with his pioneering work on onium salts, Crivello laid the foundation for the cationic curing of epoxides and vinyl ethers with photolatent acids.[4] To date, numerous photoacid generators (and appropriate photosensitizers) have been introduced, which cover a wide range of absorption characteristics, quantum yields and pK_a values of the liberated acid.[5] Whilst photolatent acids are commonly applied in technically relevant formulations, the industrial use of photolatent bases is still in its infancy.[6]

As reported in the literature, the photo-induced release of tertiary amines, tetramethylguanidines or amidine bases can be exploited to cure thiol-epoxy, thiol-Michael and epoxy resins on demand, while providing a decent storage stability at room temperature.[7] However, light triggered reactions are limited to thin films with a sufficiently high optical transmissivity (low filler and/or pigment content) to ensure an efficient activation of the catalyst over the whole cross-section of the sample.

In contrast, thermolatent bases are less affected by the sample's geometry and can be applied even in highly filled polymers or reinforced polymer composites. Depending on the molecular structure, the activation temperature can be varied

[a]*Polymer Competence Center Leoben GmbH, Sauraugasse 1, A-8700 Leoben, Austria. E-mail: sandra.schloegl@pccl.at*

[b]*Department of Polymer Engineering and Science, Technical University of Leoben, Otto Glöckel-Strasse 2, Leoben, A-8700, Austria*

[c]*Institute of Chemistry and Technology of Materials, Graz University of Technology, Stremayrgasse 9, A-8010 Graz, Austria*

[d]*University of Zagreb Faculty of Chemical Engineering and Technology, Trg Marka Marulića 19, Zagreb, HR-10000, Croatia*

over a broad range.[2] Joullié *et al.* reported on 1,3-dimethylimidazolium iodide, releasing 1-methylimidazole at temperatures above 200 °C.[8] Endo and co-workers developed various heat triggerable systems that liberate 4-aminopyridine or secondary and tertiary amines at temperatures between 120 and 190 °C.[9] In contrast, the latent aminimides, introduced by Tomita *et al.*, are able to release 1,1-dimethylamino-2-propanol already at 80 °C.[10] Generally, latent catalysts provide a versatile approach to govern the initiation and rate of polymerization in basic research and technical applications of polymers (*e.g.* preparation of ready-to-use formulations with high shelf time). Recently, they have also gained increased attention in selectively activating bond exchange reactions in dynamic polymer networks. Dynamic polymer networks emerged as promising materials for a circular polymer economy, enabling repair, reshaping, and recycling without loss of performance. Latent catalysts such as thermally activated base generators (TBGs) allow precise control over network rearrangement, enhancing reprocess-ability while avoiding premature degradation. By extending service lifetimes and enabling multiple reprocessing cycles, TBG-catalyzed vitrimers can contribute to lowering the carbon footprint of polymer production and align with broader carbon neutrality targets.[11] As previously reported, QAS-based systems enable one-time thermal activation, where the released base acts as a catalyst for bond exchange reactions.[12] 1,3,4,6,7,8-hexahydro-2*H*-pyrimido[1,2-*a*]pyrimidin-1-ium 2-cyanoacetate (TBDCA) was synthesized as a thermolatent base, efficiently releasing 1,5,7-triazabicyclo(4.4.0)dec-5-ene (TBD) at 145 °C. When incorporated into a thiol–ene network—radically cured by either light or heat—the material behaved as a permanent network until the decomposition temperature of the thermolatent catalyst was reached. In contrast, fast stress relaxation was observed at 70 °C as soon as the base was thermally liberated. The thermo-activated release of the catalyst was demonstrated by reshaping highly filled magneto-responsive polymers and fiber-reinforced polymer composites.[12] The versatility of the thermolatent bases was further demonstrated by printing 3D objects, in which the catalyst was thermally activated in selected parts. In this work, a significantly expand upon this proof-of-concept study by synthesizing a diverse and comprehensive library of thermolatent Brønsted bases tailored for use in dynamic polymer networks undergoing base-catalyzed bond exchange reactions, such as transesterification or thiol–thioester exchange.[13] The ideal thermolatent base should exhibit high stability within the operation window of the targeted application, release the catalyzing species at temperatures well above the onset temperature of dynamic bond exchange, and possess good solubility in the resin and the resulting polymer. With this in mind, the ionic TBGs were prepared in a straight-forward one-pot reaction following the salt formation between guanidine-type Brønsted bases and various carboxylic acids. To gain deeper insights into the structure–property relationships, a systematic investigation was conducted on how the nature of the base cation as well as the carboxylate anion affect the release (activation) temperature of the base. Thermal properties, including the temperature of decomposition and subsequent base release, were analyzed using thermogravimetric analysis (TGA) and differential scanning calorimetry (DSC). From these data, the activation temperatures ($T_{\text{TBG-ACT}}$) was derived for each TBG, and correlated with specific structural motifs and neighboring group effects. To further elucidate the decomposition pathways, evolved gas analysis coupled with fourier transform infrared spectroscopy (EGA-FTIR) was performed. To verify that the observed decomposition leads to the selective release of a base rather than nonspecific molecular cleavage, the change in pH value was monitored in solution. These findings demonstrate that this class of thermolatent catalysts offers a valuable strategy for extending the operational window of dynamic polymer networks. Several of the newly synthesized TBGs exhibit sufficient stability for use in high glass-transition temperature (T_g) dynamic polymer networks, such as epoxy-anhydride systems, which require curing and $T_{\text{TBG-ACT}}$ well above 100 °C. These advances mark a significant step in the transfer of dynamic covalent chemistry to technical applications such as automotive, rail, and aerospace industries.

2 Results and discussion

2.1. Concept of tailored base release

Due to their tuneable structure, catalytic efficiency in transesterification reactions, and potential for thermal latency, quaternary ammonium salts (QASs) have emerged as promising TBG candidates. Once thermally released, the liberated base can act as a catalyst for bond exchange reactions in dynamic polymer networks.[12] In previous work, cyanoacetate served as the carboxylate counter-anion, leveraging its well-documented ability to undergo thermal decarboxylation for triggering irreversible base release. Building upon this foundation, the present study explores the broader concept of thermally induced base liberation *via* decarboxylation of cyanoacetate-based QASs as a function of liberated base (*e.g.* 1,8-diazabicyclo[5.4.0]undec-7-ene, DBU; *N*,*N*,*N*′,*N*′-tetramethylguanidine, TMG; and 1,4-diazabicyclo[2.2.2]octane, DABCO).[12,14] In a further step, TBD was used as a basic building block whilst structurally diverse carboxylic acids were applied to synthesize QAS-type systems. The focus was placed on identifying alternative carboxylic acids with known thermal lability to further tune the $T_{\text{TBG-ACT}}$ and improve structural stability of the TBGs. Five distinct cleavage mechanisms for QAS-type systems are described in literature: decarboxylation,[13,15] ketonization,[16] dehydration,[16,17] condensation[16] low molecular weight cleavage,[18] and decarbonylation (Scheme S1 in SI).[19] Specifically, propanedioic acid (MA) and trichloroacetic acid (TCA) were selected in this study due to their reported varying decarboxylation temperatures of 100 °C and 80 °C, respectively.[20,21] By varying the chemical structure of the carboxylate anion, the decomposition temperature of the TBGs was tailored, thereby enabling control over the release kinetics of the base.

The air and water tolerant one-step synthesis provided the TBGs with high yields ranging from 90% to 96%. NMR and FTIR spectra were in good agreement with the proposed structures (Fig. S1–S48 in SI).

2.2. Influence of the base on the performance of cyanoacetate-based QASs

To investigate the role of the base in the cleavage mechanism and thermal release properties, **1-a** to **1-f** were synthesized (Fig. 1a). The compounds share the same anion (cyanoacetate) but are composed of different cations, which vary in terms of basicity, nucleophilicity, and steric hindrance. 2-Cyanoacetic acid (CA) was chosen as building block based on previous studies, which demonstrated its ability to undergo thermal decarboxylation and subsequent base release.[12] Compound **1-a** was utilized as a reference to compare and benchmark the newly synthesized TBGs. Fig. 1b shows schematic

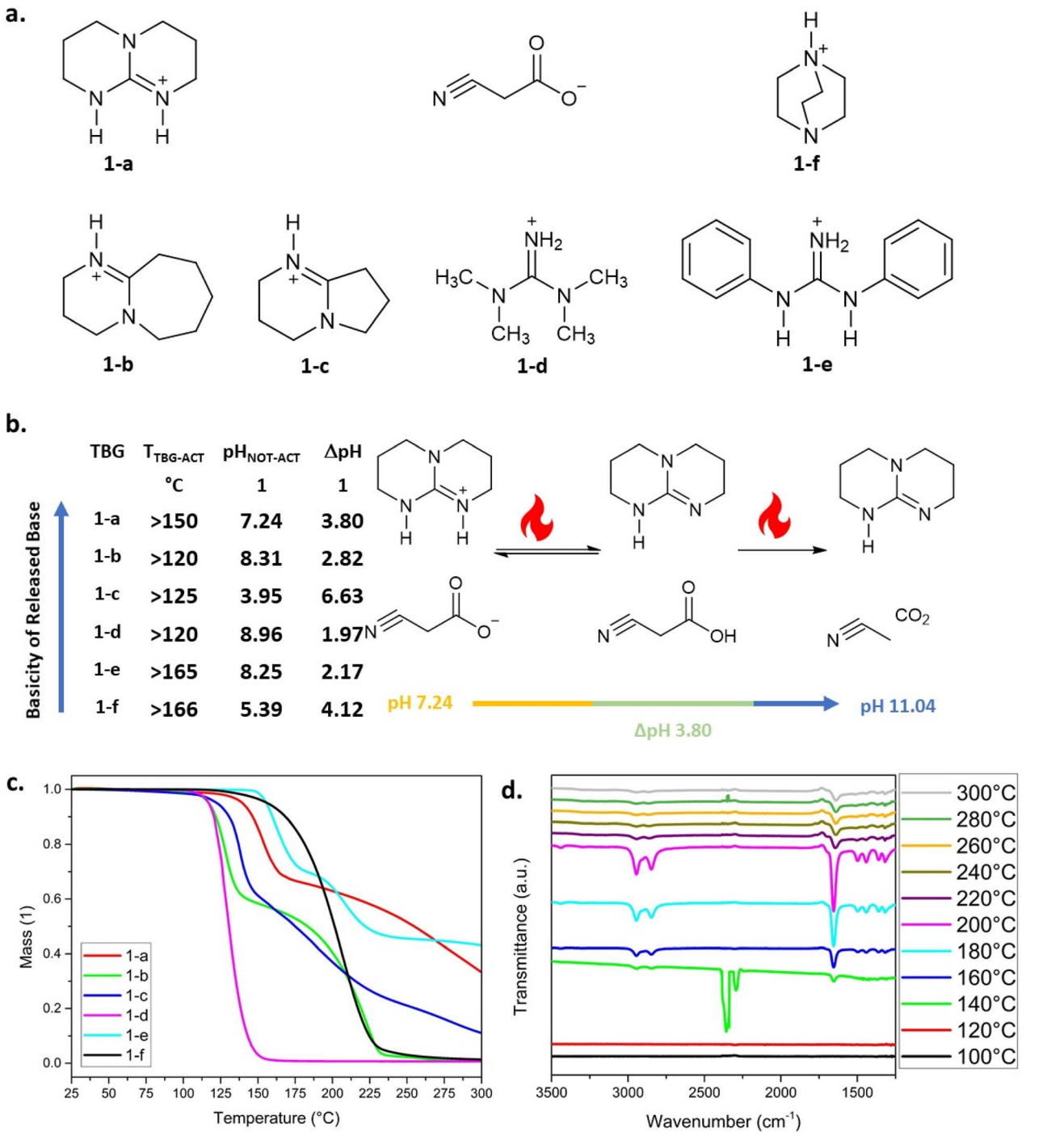

Fig. 1 Influence of the base structure on the thermal properties of cyanoacetate-based QSAs. (a) Chemical structures of the synthesized TBGs **1-a–f**. (b) Summary of $T_{TBG-ACT}$, ΔpH, and pH values in the non-activated state; schematic representation of the thermal cleavage mechanism, exemplified by **1-a** and the related pH change during base release. (c) TGA analysis of the TBGs **1-a–f**. (d) EGA-FTIR analysis during thermal decomposition of **1-a**.

representation of the thermal cleavage process and base release, using **1-a** as an example, along with the observed pH-shift (ΔpH). TGA analysis of the synthesized compounds was carried out to determine their $T_{TBG\text{-}ACT}$, which is defined as the temperature at which the compound exhibits a mass loss higher than 3 wt% (Fig. 1b). The trend observed for the thermal stability of the TBGs, ranked by their $T_{TBG\text{-}ACT}$ from highest to lowest, is as follows: **1-f** > **1-e** > **1-a** > **1-c** > **1-b** > **1-d**.

Comparing the data with the pK_a values of the released base, it is obvious that $T_{TBG\text{-}ACT}$ does only partially correlate with their basicity: **1-a** > **1-b** > **1-c** > **1-d** > **1-f** > **1-e**.[14] Among structurally similar compounds (**1-a** to **1-d**), all of which contain an amidine base in their structure, **1-b** and **1-c** do not follow the expected trend. Despite having similar basicity, **1-b** has a lower $T_{TBG\text{-}ACT}$ than **1-c**. This indicates that factors beyond basicity influence the thermal stability of the TBGs. Notably, although **1-b** and **1-c** share an amidine core, **1-b** contains a seven-membered ring, whereas **1-c** features a five-membered one. The literature suggests that this structural difference alters nucleophilicity,[22] with the five-membered ring in **1-c**, leading to slightly higher thermal stability compared to **1-b**. Consequently, increased nucleophilicity may contribute to an enhanced thermal stability, at least in compounds with comparable basicity. The influence of nucleophilicity may also partly explain the high thermal stability of **1-f**. In contrast to **1-a** and **1-d**, where the nitrogen lone pair participates in a conjugated system, **1-f** possesses two equivalent nitrogen centers, leading to charge delocalization.[23] This unique electronic distribution is likely to stabilize the bound complex, thereby increasing the cleavage temperature of the corresponding TBG. Additionally, the bicyclic nature of the cation in **1-f** introduces a rigidity, contributing to steric effects that further enhance thermal stability.[24] Recent work has shown how steric constraints interplay with dispersion forces to impact the spatial arrangement and therefore stabilization in rigid, π-delocalized frameworks.[25] Finally, the thermal behavior of **1-e** warrants discussion. Unlike **1-d**, which features a base with two methyl groups as substituents, the guanidine base in **1-e** contains two phenyl rings. Thermal analysis indicates that **1-e** exhibits a higher $T_{TBG\text{-}ACT}$ than **1-d**. According to literature,[20] **1-e** has a lower basicity than **1-d** and should therefore be less thermally stable. However, despite containing a guanidine structure, **1-e** deviates from the expected trend. This suggests that the phenyl substituents exert a more significant influence on thermal stability than basicity. The increased stability of **1-e** might be attributed to steric hindrance, as the bulky diphenyl groups shield the active site from undesired interactions.[26] Additionally, π–π interactions between the phenyl rings may contribute to electronic stabilization, further explaining the unexpectedly high thermal stability of this TBG.[27] During thermal activation, two distinct thermal decomposition trends can be observed in the TGA curves, which become particularly evident in the derivative thermogravimetric (DTG) analysis and can be further examined using DSC (Fig. S2–S12 in SI). A two-step decomposition is observed for compounds **1-a**, **1-b**, **1-c**, and **1-e**, whereas a one-step decomposition is characteristic of **1-d** and **1-f**. For compounds exhibiting a two-step decomposition pattern, the boiling of the base exceeds $T_{TBG\text{-}ACT}$ (Fig. S13 in SI provides the TGA curves of the pure bases used in this study). Consequently, the second step can be attributed to the continuous evaporation of the released base. This suggests that the first decomposition step is driven by a chemical reaction (activation of the TBG), whereas the second step corresponds to a purely physical process (evaporation of the liberated base). This hypothesis is further supported by DSC and DTG analysis, where two distinct peaks can be observed for **1-a**, **1-b**, **1-c**, and **1-e**. The first peak, corresponding to the cleavage of the stabilization group, is sharp and well-defined, indicating a sudden chemical reaction. In contrast, the second peak appears broader, consistent with a gradual physical evaporation process. A one-step process, on the other hand, occurs when the $T_{TBG\text{-}ACT}$ is within a narrow range close to or even exceeding the initial mass loss/boiling point of the base. Under these conditions, the physical evaporation of the base occurs immediately after the cleavage of the carboxylate anion, preventing the distinct separation of chemical activation and evaporation. This behavior is evident in both DTG and DSC curves of **1-d** and **1-f**. A similar deactivation behavior has also already been observed in a previous study on photo-latent catalysts.[28] In this scenario, after initial photoactivation, rapid evaporation of the base resulted in the loss of catalytic anion.

EGA-FTIR confirmed that the first cleavage step involves the decomposition of the cyanoacetate into CO_2 and acetonitrile, followed by the non-destructive evaporation of the released base (Fig. 1d, S2–S12 in SI). This stepwise behavior was observed for all TBGs investigated within this series. However, variations between compounds were detected, consistent with previous TGA results. Specifically, **1-a**, **1-b**, **1-c**, and **1-e**, which previously exhibited a two-step decomposition pattern in TGA, displayed a similar behavior in EGA-FTIR. In these cases, an initial CO_2 signal was observed, followed by the detection of the liberated base at higher temperatures. In contrast, for **1-d** and **1-f**, the spectral signals of CO_2 and the base overlapped, supporting the earlier hypothesis that, evaporation of the base occurs immediately after decarboxylation. This behavior is exemplified by the EGA-FTIR data of **1-a**, where an infrared (IR) transmittance signal appeared at 2334 cm^{-1} at temperatures starting from 150 °C, consistent with literature reports on CO_2.[29] Upon further temperature increase, additional peaks emerged at 3450, 2950–2850, 1650, 1490–1440 and 1360–1325 cm^{-1}, which can be attributed to the released TBD (FTIR of pure bases and EGA-FTIR of pure TBD are provided in Fig. S13–S20 in SI). Comparing the EGA-FTIR data of the TBGs in this series, it can be concluded that the choice of base influences the $T_{TBG\text{-}ACT}$, although the fundamental cleavage mechanism remains unchanged.

To confirm that the observed cleavage is not merely a result of thermal degradation of the compound, but rather a selective base release, pH-measurements were performed prior to and after thermal activation **1-a–f** (Tables S5–S10 in SI). The experiments were conducted in a 3 mL DMSO/19 mL deionized water mixture at a concentration of 1 mmol L^{-1}, following a heating protocol kept constant for all TBGs in this series. Each pH value represents the mean of three replicate measurements, and

standard deviations were ≤0.05 pH units. The pH-measurements were conducted in solution (mixture of DMSO and water) following a heating protocol, which kept constant for the TBGs in this series (see experimental procedure in SI). Using compound **1-a** as a reference, experiments were performed to determine the lowest temperature at which base release occurred and the conditions at which the largest ΔpH was observed (see SI Table S5 for full protocol and reproducibility details). The uncertainty in activation temperature in solution ($T_{pH\text{-}ACT}$) values was estimated at ±2 °C, based on replicate runs and instrument calibration. Remarkably, significant base release was already observed for **1-a** even after 1 hour of heating at 40 °C, despite both EGA-FTIR and TGA analyses indicating thermal stability up to 150 °C. This suggests that the thermal stability of the TBG strongly depends on whether it is measured in solid state or in solution. A maximum shift in pH value was obtained at 140 °C for 30 minutes, which corresponds well with the decarboxylation temperature of CA reported in the literature.[12] Under these conditions, a ΔpH of 3.96 was achieved, which is comparable to the ΔpH of 3.80 observed after activation at 200 °C for 1 hour (Fig. 1b). These results highlight the efficient and clean activation of **1-a** across a broad temperature range. To assess the reduction in basicity over time, pH-measurements were repeated after 36 days of storage at room temperature using compound **1-a**. Prior to storage, **1-a** was thermally activated under experimental conditions (200 °C, 1 h). No significant difference in pH was observed between the freshly prepared and stored samples (see SI Table S25). For subsequent studies, thermal activation of TBG solutions were conducted at 200 °C for 1 h. All tested TBGs (**1a–f**) exhibited a significant increase in basicity upon thermal activation. Control experiments confirmed that both DMSO and all free bases are thermally stable at 200 °C for at least one hour, thereby excluding their decomposition as contributing factors to the observed ΔpH (see experimental procedure in SI). Once thermally activated, the TBG solutions exhibited pH values comparable to those of liberated bases (Table S4 in SI) at identical concentrations. This confirms the efficiency of base release using CA as stabilization group. After analyzing the ΔpH values and the pH of the not-activated state ($pH_{NOT\text{-}ACT}$), two distinct trends were observed for compounds **1-a** to **1-f** (see SI Tables S5–S10). $pH_{NOT\text{-}ACT}$ follows the trend: **1-d** > **1-b** > **1-e** > **1-a** > **1-f** > **1-c**. In contrast, the ΔpH values follow the opposite trend: **1-c** > **1-f** > **1-a** > **1-b** > **1-e** > **1-d**. With the exception of compounds **1-b** and **1-e**, whose ΔpH are minor (<0.2), these trends are nearly inverse to each other. Importantly, they do not align with the known basicity of the liberated bases.[14] Compounds **1-a**, **1-b**, **1-d**, and **1-e** exhibit moderately basic pH values between 7.24 and 8.96 in their non-activated state. Notably, similarly structured compounds (**1-a**, **1-b**, and **1-d**) demonstrate a trend of increasing $pH_{NOT\text{-}ACT}$ with decreasing basicity. Despite this, compounds **1-c** and **1-f** show significantly more acidic pH values (3.95 and 5.39), but upon thermal activation exhibit the largest thermal activation ΔpH of 6.63 and 4.12, respectively. Here, the pH value of the activated TBGs are in good agreement with those of the free bases, DBN and DABCO.[22,30] These observations reveal that the nucleophilicity of the base governs the pH value of the not-activated TBG. Higher nucleophilic cations generally lead to lower (more acidic) pH values. In contrast the basicity of the cation plays a minor role. However once thermally activated, the TBG solutions reach pH values that closely resemble those of the corresponding free bases. Thus, in the case of TBGs containing highly nucleophilic cations, the activation process results in particularly large ΔpH.

To better understand which cation-dependent molecular factors influence the thermal activation behavior of TBGs, a multivariate correlation analysis was conducted using compounds **1-a-f**. The target parameter was $T_{TBG\text{-}ACT}$ (solid state) obtained from TGA experiments. Several experimentally accessible descriptors were used as independent variables: the base strength pK_B (measured in acetonitrile),[14] ΔpH, and $pH_{NOT\text{-}ACT}$. Additionally, two qualitative structural parameters, nucleophilicity and steric hindrance, were introduced and numerically ranked from 1 to 5 based on literature values and structural evaluation, allowing these factors to be included in the correlation analysis.

Nucleophilicity rankings were taken from reactivity scales reported in literature, placing DABCO and TBD as the most nucleophilic ones, followed by 1,5-diazabicyclo[4.3.0]non-5-ene (DBN), DBU, and TMG.[22,31] However, literature data on *N*,*N*′-diphenylguanidine (DPG) was lacking. It was assigned to a low nucleophilicity score based on resonance delocalization into aryl groups, which dampens electron availability.

Steric hindrance was ranked structurally, with compact, symmetric bases such as DABCO receiving low scores (1), and bulkier, branched or aromatic systems such DPG or TMG receiving high scores (5). Only correlations between individual descriptors and $T_{TBG\text{-}ACT}$ are discussed in the main text for clarity. The full Pearson correlation matrix is provided in the SI (Table S27), allowing assessment of interdependencies between all variables. The input parameters are shown in Table S26.

The Pearson correlation analysis revealed several key insights into how these parameters influence $T_{TBG\text{-}ACT}$: The strongest correlation with $T_{TBG\text{-}ACT}$ was observed for ΔpH ($r = -0.99$) and $pH_{NOT\text{-}ACT}$ ($r = -0.99$). This suggests that compounds with a higher initial pH and a smaller pH change upon activation require lower energy input for cleavage, likely due to a more loosely bounded base.

pK_B showed a strong positive correlation ($r = +0.94$) with $T_{TBG\text{-}ACT}$, indicating that stronger bases (higher pK_B) form more stable salts with cyanoacetate, requiring more energy for cleavage. Nucleophilicity exhibited a moderate negative correlation ($r = -0.79$). More nucleophilic bases tend to cleave at lower temperatures, likely because their greater electron-donating character destabilizes the ionic salt and facilitates dissociation. This supports the idea that reactivity of the cation is a driving factor in salt decomposition, independent of just pK_B. Steric hindrance, in contrast, exhibited negligible correlation ($r = +0.22$). This may be due to the relatively rigid structures of the bases studied or due to solvation and packing effects that minimize steric impact.

These results highlight that $T_{TBG\text{-}ACT}$ in this series is strongly governed by acid–base equilibrium descriptors (pK_B, $pH_{NOT\text{-}ACT}$, ΔpH) and nucleophilic character, while steric effects play

a minor role. Notably, the semi-empirical rankings of nucleophilicity and steric hindrance, while qualitative, aligned well with expected trends and contributed meaningfully to the interpretation of thermal behavior. Collectively, these findings emphasize that cation variation is a powerful strategy for modulating the activation behavior of TBGs. This has implications for the design of future catalytic systems, especially where selective base release or compatibility with polymer networks is desired.

2.3. Influence of neighboring group effects in the anion on the thermal stability of QASs

To investigate the effect of substituents on the cleavage mechanism and thermal release behavior a series of acetate-based TBG derivatives (**2-a–g** and **1-a**) were synthesized (Fig. 2a). All compounds featured TBD as basic building block, while the anionic counterparts were structurally derived from acetic acid analogues with chloro, cyano, hydroxy, methyl, and oxo groups. Additionally, the effect of multiple substituents on the thermal behavior was explored. The parent acetate-based TBG (**2-a**) was employed as a reference compound to assess the impact of each substituent on thermal stability. The systematic variation of anionic substituents among derivatives **2-a–g** and **1-a** enabled a detailed analysis of the structure–property relationships governing the thermal decomposition profiles of the compounds. According to TGA analysis thermal stability of the TBGs bearing a single substituent group follows the descending order: **2-b** > **2-c** > **2-a** > **1-a** (Fig. 2b and c). Among these, compound **2-b**, which contains a chlorine substituent, exhibits the highest thermal stability. This enhanced stability can be attributed to the moderate electron-withdrawing inductive effect (−I) of the chlorine group, which stabilizes the carboxylate form and reinforces the adjacent C–C bonds without overly activating the system. Moreover, the absence of a nucleophilic side group further increases its thermal stability. The second most thermally stable compound is **2-c**, which features a hydroxyl group as a substituent. Hydroxyl groups are reported to engage in intramolecular interactions with the carboxylic acid moiety, potentially forming cyclic intermediates at elevated temperatures and thereby reducing the overall thermal stability.[32,33] Although compound **2-c** shows a slightly higher $T_{TBG\text{-}ACT}$ (>243 °C) compared to **2-b** (>230 °C), compound **2-b** demonstrates a slower and more gradual mass loss at elevated temperatures, indicating a more extended resistance to complete thermal decomposition. The relatively high thermal stability of **2-c** can be attributed to the hydroxyl group at the α-position exerting an electron-donating mesomeric effect (+M), which stabilizes both the α-carbon and the carboxylate moiety through resonance delocalization. Unlike cyanoacetates or trichloroacetates, which readily undergo decarboxylation due to strong electron-withdrawing substituents, the hydroxyl group is not a potent electron-withdrawing group. As a result, the formation of a carbanion intermediate is less favored at lower temperatures, avoiding premature thermal activation due to the absence of strong −I or −M effects.[34–36] Additionally, compound **2-c** contains both hydroxyl and carboxylic acid groups.

While the –OH group can contribute to thermal stability through intramolecular or intermolecular hydrogen bonding at lower temperatures, it also introduces a risk of thermally induced side reactions at elevated temperatures. These may include intramolecular esterification or lactonization, which compromise on structural stability.[37] Finally, the acidity of the parent acid from which the anion is derived may also influence the thermal behavior. The corresponding acid from **2-b** is slightly more acidic than that of **2-c**. In general, a more acidic species tends to form a more stabilized conjugated acid when structural backbones are comparable. Stronger electrostatic attraction can delay thermal decomposition resulting in a higher $T_{TBG\text{-}ACT}$ of **2-b**.[38] **2-a** is characterized by a lower thermal stability than **2-c**. The absence of hydrogen bonding makes the molecule more prone to cleavage at lower temperatures. On the other hand, the methyl group is weakly electron donating *via* the +I effect, leading to a lower $T_{TBG\text{-}ACT}$.[38] Among the investigated compounds, **1-a**, bearing a cyano substituent, exhibits the lowest thermal stability, as the nitrile group is a strongly electron-withdrawing substituent. The −I effect withdraws electron density through σ-bonds, while the -M effect stabilizes adjacent carbanionic intermediates *via* resonance.[39] These combined electronic effects are expected to destabilize the α-carbon and weaken the structural integrity of the compound, thereby facilitating decarboxylation. In addition, the decarboxylation reaction yields thermodynamically stable products such as acetonitrile and CO_2, which further drives the decomposition process forward under thermal conditions. This overall effect contributes significantly to the lower $T_{TBG\text{-}ACT}$ observed for compound **1-a**.[40] The significantly higher $T_{TBG\text{-}ACT}$ of **2-b** compared to **2-d** can be related to the nature and number of electron-withdrawing substituents.

2-b contains a single chlorine substituent, whereas **2-d** bears a trichloromethyl group, which exerts a strong –I effect.

Destabilization of the C–C bond between the α -carbon and the adjacent carboxylic group lowers the energy barrier for decomposition reactions, particularly decarboxylation. In contrast, the mono-chloro substituent in **2-b** exerts a comparatively moderate –I effect. As discussed previously, this milder electron-withdrawing character contributes to a more balanced stabilization of the molecule, reinforcing bond strength and thereby enhancing $T_{TBG\text{-}ACT}$.[41,42] In further experiments, TBGs were synthesized with pairs of hydroxy, oxo, and methyl groups, and their effect on the thermal stability was analyzed. TGA analysis revealed that $T_{TBG\text{-}ACT}$, follows the descending order: **2-e** > **2-f** > **2-g**. **2-e** (Fig. 2d and e), which contains both a hydroxy and a methyl group, exhibits the highest $T_{TBG\text{-}ACT}$ among the three compounds. The methyl group increases electron density on the anionic moiety and stabilizes the structure by decreasing its susceptibility to nucleophilic attack. In contrast, the electron withdrawing hydroxy group further stabilizes the TBG, making it less prone to decomposition. Together, the opposing effects of the hydroxy and the methyl group work synergistically to enhance the thermal stability of **2-e**. The hydroxy group contributes to the overall structural stabilization, while the methyl group reduces the propensity for decomposition at higher temperatures.[43,44] In **2-f**, the strong electron withdrawing

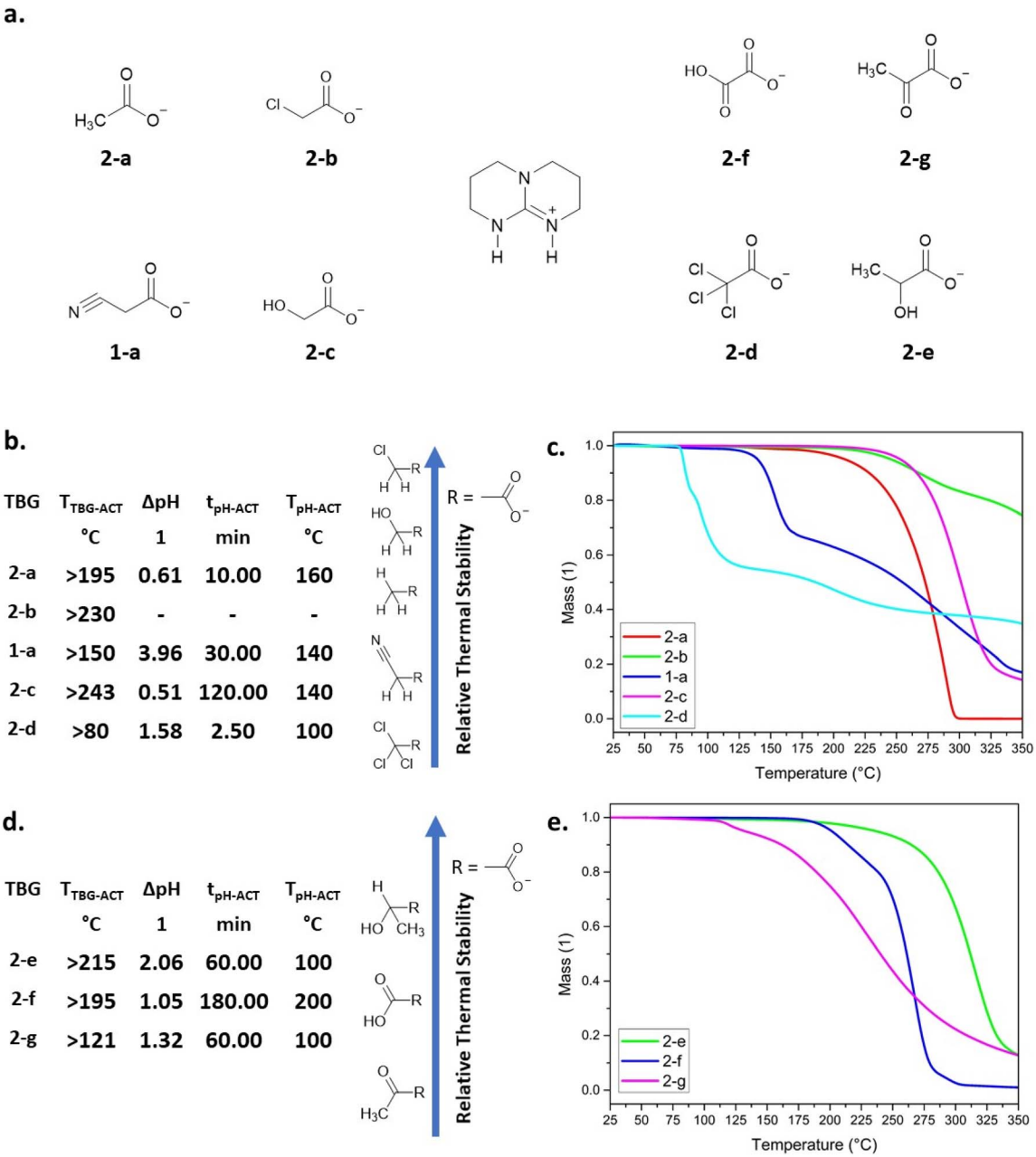

Fig. 2 Influence of different stabilization groups from acetate derivatives on the properties of TBD releasing QASs. (a) Chemical structures of the synthesized TBGs **2-a–g**. (b and d) Summary of $T_{TBG-ACT}$, ΔpH after activation, t_{pH-ACT}, and T_{pH-ACT}; including a schematic representation of the relative thermal stability of the acetate derivatives. TGA analysis of the TBGs (c) **1-a**, **2-a–g** and (e) **2-e–g**.

oxo group decreases electron density on the anion, making it more electrophilic and reactive. This increased electrophilicity reduces the thermal stability of the TBG.[45] Similarly to compound **2-e**, the hydroxy group in **2-f** also exerts an −I effect. However, the electron-withdrawing influence of the hydroxy group is counteracted by the strong electron-withdrawing effect of the oxo group. This interplay results in a destabilizing effect by increasing the electron deficiency of the anion, making it more susceptible to nucleophilic attack and subsequent cleavage. In contrast, the methyl group in **2-e** donates electron density *via* its inductive effect, which stabilizes the TBG to a certain extent and contributes to the slightly higher thermal stability of **2-e** compared to **2-f**.[45] Among the three compounds, **2-g** containing an oxo group and a methyl group as substituents exhibits the lowest thermal stability. Here, the stabilizing influence of the methyl group seems to be not sufficient enough to counteract the strong destabilizing effect imposed by the oxo group.[46] In addition, the absence of hydrogen bonding and other stabilization effects might explain the lower thermal stability of **2-g** compared to **2-f**. To further analyze the thermal cleavage behavior. For **1-a** and **2-a–g** EGA-FTIR was employed (Fig. S21–S34). Four distinct decomposition profiles were

identified. Analogues to **1-a**, **2-d**, **2-f**, and **2-g** exhibited a stepwise thermal activation pattern. An initial release of CO_2 at 2334 cm^{-1} was followed by the evaporation of TBD, evident from the characteristic IR bands at 3450, 2950–2850, 1650, 1490–1440, and 1360–1325 cm^{-1}, matching those of the pure base (Fig. S20 in SI) Additionally **1-d** exhibited a band at 1250 cm^{-1} indicating the formation of chloroform and subsequently clean cleavage. Notably, **2-f**, which released CO_2 between 180 and 220 °C, showed a delayed base release compared to pure TBD, indicating thermal stabilization of the salt form. In contrast, compounds **2-c** and **2-e** demonstrated a simultaneous release of CO_2 and TBD beginning at 240 °C, which is significantly higher than the base's volatilization temperature. This suggests enhanced thermal stability in the solid state, consistent with TGA results. Additionally, both compounds showed new bands between at 3400–3000, 1575 and 1200 cm^{-1} and enhanced signals at 1360 and 1325 cm^{-1}. These spectral changes are attributed to the presence of α-hydroxy acids in **2-c** and **2-e**, which upon decarboxylation release aldehydes[47] (*e.g.*, formaldehyde or acetaldehyde) that may condense with TBD, explaining the sustained intensity of TBD-related peaks up to 360 °C. **2-b** also showed a distinct CO_2 release between 240–280 °C. However, subsequent TBD-related signals were partially suppressed: the 1360–1325 cm^{-1} region vanished and the 1490–1440 cm^{-1} bands weakened. In their place, broad peaks between 3410–3000 cm^{-1}, along with new signals at 1315, 1285, and 1050 cm^{-1}, were observed. These are consistent with N-alkylation or condensation reactions between TBD and chlorinated side products formed after decarboxylation of the chloroacetate.[48] Finally, **2-a** exhibited no detectable CO_2 release. Instead, a slight-broad water band between 3000–3400 cm^{-1}, a new doublet between 1800–1750 cm^{-1} and a strong band at 1160 cm^{-1} were observed concurrently with the typical TBD peaks. These features correspond to the *in situ* formation of acetic anhydride,[49] suggesting that cleavage occurs *via* a condensation mechanism between two acetate units, catalyzed by the basic TBD environment.

To further quantify the base release of the TBGs, the temperature ($T_{pH\text{-}ACT}$) and time ($t_{pH\text{-}ACT}$), defined as the conditions under which the highest ΔpH (*i.e.* maximum base release) was observed, were determined by pH-measurements in 3 mL DMSO/19 mL deionized water solution at a concentration of 1 mmol L^{-1} (full protocol in SI). Measurements were performed in triplicate, and the uncertainty in $T_{pH\text{-}ACT}$ values is ± 2 °C. The samples were thermally treated at a defined temperature for a fixed time (or *vice versa*), and the ΔpH was calculated by subtracting the pH of the non-activated solution from the pH of the activated solution (see SI Tables S11–S17). Interestingly, all TBGs in this series demonstrated a distinct, non-linear pH activation profile, characterized by a narrow thermal window where the ΔpH was maximized. This suggests that base release is governed by a delicate interplay of thermally triggered cleavage (*e.g.*, decarboxylation) and the onset of competing side reactions that deactivate the liberated base or yield phenolic byproducts.[50] Each compound exhibited a $T_{pH\text{-}ACT}$ and $t_{pH\text{-}ACT}$, directly correlating with its structural features and inherent thermal stability (see Fig. 2b and d). These results highlight the critical role of acid selection in maintaining pH stability post-activation. Specifically, CA as stabilization group showed clean cleavage, without further side reactions, and therefore a sustained basicity with negligible decomposition of the released base over time. Recent studies have further revealed that guanidine-based cations, are able to undergo ring-opening reactions in aqueous environments, leading to a significant reduction in the observed ΔpH upon thermal activation.[51] This observation is consistent with the experimental conditions, as all pH-measurements were conducted in water-containing media. In particular, the thermal activation process involves two concurrent reactions: the intended, thermally triggered base release and a competing ring-opening side reaction, which is accelerated under elevated temperatures and in the presence of water. The extent of pH suppression is further affected by the decomposition behavior of the carboxylate itself. CA, which follows clean and well-defined cleavage pathways, do not show evidence of this ring-opening behavior. This can be attributed to its rapid and selective decomposition, which occurs prior to any significant ring-opening of the guanidinium species. As a result, the thermally liberated base remains stable in the DMSO/H_2O solution, and the overall ΔpH is preserved. Across the examined compounds, four distinct activation behaviors emerge. For **1-a**, the pH activation begins already at 80 °C after 30 min, after which the ΔpH remains stable and constant with only small changes in pH even after 5 hours at 200 °C (see SI Table S5). Its relatively high ΔpH (3.96) suggests that most of the released base is pH-active and not sequestered or decomposed as already discussed in the previous section. In contrast compounds having dual substituents (**2-e**, **2-f**, and **2-g**) show a clean and moderate base release after reaching their $t_{pH\text{-}ACT}$ and $T_{pH\text{-}ACT}$. Increasing $T > T_{pH\text{-}ACT}$ has only limited impact on the basicity. Slight ΔpH can also occur before reaching $T_{pH\text{-}ACT}$. However, extending the duration of activation at increased temperatures (*e.g.* 200 °C) leads to a clear decrease in basicity. Mono-substituted acetic acid derivatives (**2-a**, **2-b**, and **2-c**) exhibit low or even ΔpH toward higher acidity. For example, **2-b** becomes more acidic upon activation, which may be due to the formation of acidic decomposition products (*e.g.* HCl). Similarly, **2-c** shows a reduction in pH upon extended heating, suggesting base decomposition or capture. In contrast **2-d** demonstrates efficient base release and reaches a moderate ΔpH of 1.58 at its $t_{pH\text{-}ACT}$ and $T_{pH\text{-}ACT}$. However, upon prolonged thermal treatment, **2-d** shows a significant reduction in basicity, indicating possible decomposition of the released base or buffering by decomposition products. Furthermore, in this series, **2-a**, **2-c**, and **2-e** exhibited significant ΔpH at temperatures far below $T_{TBG\text{-}ACT}$ (Fig. 2b and d), which aligns well with the in the previous chapter discussed results for **1-a**. For example, compound **2-e** starts to activate in solution already at temperatures as low as 100 °C, despite its $T_{TBG\text{-}ACT}$ at 215 °C in the solid state. Also share **2-c** and **2-e** structurally both a free hydroxy group, which may support this behavior. In contrast **2-d** and **2-f** show activation in solution at temperatures at or above $T_{TBG\text{-}ACT}$ (Fig. 2b and d). This further supports the idea, that the thermal stability of the TBGs is highly dependent on if they are in solid state or solution. Furthermore, the chemical structure

of the anion of the TBG and interactions with solvents might also have impact on the thermal stability of the compound in solution. For example, **2-a**, **2-e**, and **2-g** feature a methyl-substituted anion, which may contribute to a reduced thermal stability in DMSO/water mixtures due to structural similarities that favor premature activation or decomposition under these conditions. A behavior that has also been reported in previous studies for electron-poor, nucleophilic anions in polar aprotic solvents.[52] These findings emphasize the importance of thermolysis stability, anion design, and base-product compatibility when tailoring TBGs for pH-controlled applications. Furthermore, it should be noted that $T_{TBG\text{-}ACT}$ and $T_{pH\text{-}ACT}$ can differ significantly. This highlights that the thermal stability of TBGs in solution can vary markedly from that of their solid-state counterparts. Consequently, in future applications involving polymeric systems, the $T_{TBG\text{-}ACT}$ of embedded TBGs may be influenced by the polymer network used.

To better understand which molecular factors influence the thermal activation behavior of TBGs, a multivariate correlation analysis was conducted for **1-a** and **2-a-g**. The target parameter was the experimentally determined $T_{TBG\text{-}ACT}$ (solid state). Several experimentally accessible and semi-quantitative descriptors were used as independent variables: pK_a (taken from literature)[53] of the acetate derivatives, molecular weight (M_W) of the salt, ΔpH, and $pH_{NOT\text{-}ACT}$. Additionally, three qualitative structural parameters were introduced and ranked numerically from 1 to 5 to enable correlation. In the first step, the decarboxylation behavior, based on EGA-FTIR profiles was taken: A value of 5 represents clean, two-step decomposition with separate CO_2 and base release; 3 indicates overlapping CO_2/base release and the formation of side products whilst 1 reflects a non-decarboxylative cleavage pathway.

In addition, inductive effects of substituents on the acid were ranked from 1 (strong –I, *e.g.*, $–CCl_3$) to 5 (strong +I, *e.g.*, alkyl or hydroxyl groups), reflecting electron withdrawal/donation at the cleavage site.

Finally, steric hindrance, reflecting spatial bulk around the anionic center was ranked from 1 (minimal hindrance, *e.g.*, acetate) to 5 (bulky groups like trichloromethyl), based on size and substitution pattern.

Only correlations between individual descriptors and $T_{TBG\text{-}ACT}$ are discussed in the main text for clarity. The full Pearson correlation matrix is provided in the SI (Table S29), allowing assessment of interdependencies between all variables. The input parameters are shown in Table S28.

The Pearson correlation analysis revealed several clear and mechanistically consistent relationships between $T_{TBG\text{-}ACT}$ and the molecular descriptors. Among the strongest correlations was pK_a ($r = -0.94$), showing that more acidic anions (lower pK_a) are associated with significantly lower $T_{TBG\text{-}ACT}$. Notably, M_W of the TBGs exhibited a strong negative correlation ($r = -0.93$) with $T_{TBG\text{-}ACT}$, indicating that smaller molecules tend to decompose more readily, likely due to reduced thermal stability and more facile diffusion.

The maximum ΔpH observed upon heating in DMSO also correlated positively with $T_{TBG\text{-}ACT}$ ($r = +0.77$), suggesting that compounds showing strong base release effects may require slightly higher energy input, possibly due to slower or more complete deprotonation. Similarly, $pH_{NOT\text{-}ACT}$ showed a moderately strong positive correlation ($r = +0.90$), implying that TBGs, which already exhibiting basic character in their unactivated form, tend to release the base only at higher temperatures. This could reflect increased ion pairing or residual basicity delaying full cleavage. Among the ranked structural parameters, the decarboxylation score revealed a highly negative correlation ($r = -0.94$) with $T_{TBG\text{-}ACT}$. This supports the hypothesis that clean, well-defined CO_2-releasing mechanisms are favorable for achieving low activation temperatures. In contrast, the inductive effect (I effect) of substituents correlated positively ($r = +0.64$) with $T_{TBG\text{-}ACT}$, indicating that electron-donating groups slightly stabilize the salt structure, delaying thermal decomposition. Steric hindrance, despite being qualitatively assessed and ranked, showed minimal correlation ($r = +0.06$) and appears to play a minor role in influencing thermal cleavage within this specific series.

In summary, the analysis reveals that electronic factors (pK_a, I effect, $pH_{NOT\text{-}ACT}$), mechanistic behavior (decarboxylation), and M_W are key contributors to thermal activation behavior. The high consistency between qualitative descriptors and experimental data supports their use in predictive modeling and rational TBG design.

To further substantiate the observed discrepancy between $T_{TBG\text{-}ACT}$ in the solid state and $T_{pH\text{-}ACT}$ in solution, activation energies by Kissinger analysis from variable heating rate experiments were determined.[54] Compounds **1-a** (cyanoacetate-based) and **2-d** (trichloroacetate-based) were selected for this study because they exhibited clean decarboxylation and strong base release (ΔpH), as previously confirmed by EGA-FTIR and pH experiments. This ensures that the measured thermal events can be directly attributed to the intended decomposition pathway, without interference from competing side reactions.

For the solution-state measurements, 100 mg of TBG were dissolved in 0.5 mL of DMSO and subjected to thermal analysis at heating rates between 5 and 35 K min^{-1} (in 10 K increments). Solid-state experiments were performed for TBG powders under otherwise identical heating protocols. Onset temperatures for Kissinger analysis were determined from the TGA curves at the respective heating rates (see experimental part and Fig. S49–S54 in SI).

The results show a consistent and pronounced difference between the two environments for both **1-a** and **2-d**. For **1-a**, the activation energy (E_a) in solution (DMSO) was determined as 52 ± 29 kJ mol^{-1}, whereas in the solid state a significantly higher value of 140 ± 21 kJ mol^{-1} was obtained. Similarly, **2-d** exhibited a solution-phase activation energy of only 28 ± 9 kJ mol^{-1}, compared to 143 ± 7 kJ mol^{-1} in the solid state. Importantly, the error ranges of solution and solid-state values do not overlap, confirming that these differences are statistically significant (Fig. S55–S58, Tables S32–S35 in SI).

These findings provide quantitative evidence for the mechanistic divergence of activation in the two environments. In DMSO solution, the apparent activation barrier is reduced due to solvation effects, stabilization of transition states, and facilitated proton transfer pathways.[55] As a result, decomposition

can occur at lower apparent onset temperatures, which is reflected in the experimentally determined $T_{pH\text{-}ACT}$. By contrast, in the solid state no such stabilization is available, and decomposition must proceed *via* direct bond scission in a constrained matrix, leading to a substantially higher activation energy and a correspondingly higher onset temperature $T_{TBG\text{-}ACT}$. The clear distinction in E_a values thus substantiates that the discrepancy between $T_{TBG\text{-}ACT}$ and $T_{pH\text{-}ACT}$ is not a methodological effect, but rather an intrinsic property of the activation mechanism in different phases. This quantitative analysis extends our earlier qualitative interpretation and provides a solid framework to understand why activation in solution (DMSO) and in the solid state follow different thermal thresholds.

2.4. Effects of degree of neutralization and carbon spacer length on the anion on the thermal stability of QASs

To investigate the effect of chain length and degree of neutralization on the cleavage mechanism and thermal release behavior of QASs, a series of dicarboxylate-based TBG derivatives were synthesized (Fig. 3a). All compounds featured TBD as basic building block, while the anionic counterparts were structurally derived from dicarboxylic acids with varying chain lengths. Depending on the stoichiometry, the dicarboxylic acids were either partly (**2-f**, **2-h–j**) or fully neutralized (**2-k–n**).

With the exception of **2-h**, the thermal stability of the partly neutralized TBGs rises with increasing chain length of the dicarboxylic acids: **2-j** > **2-i** > **2-f** > **2-h** (Fig. 3b and c). The higher thermal stability can be explained by lower electrostatic repulsion between the acid and the base moieties, lower conformational strain, enhanced flexibility in the longer-chain mono substituted acetic acid derivatives, and an increased entropic cost for cyclization or decomposition, thus raising the activation barrier for thermal cleavage.[56,57]

The low stability of the MA-based TBG (**2-h**) might be related to a different decomposition mechanism. MA is a beta-keto acid which facilitates beta-decarboxylation through carbanion stabilization of the transition state.[58] Furthermore, the TGA-curve of **2-i** (succinate) shows a minor mass loss event beginning at around 135 °C. This is either due to the loss of physisorbed or loosely bound water, or a minor initial decarboxylation reaction.[59] Whilst the partly neutralized TBGs show one major weight loss in the TGA curves the fully neutralized ones exhibit a distinct two-step weight loss.

The first mass loss occurs below 80 °C for all compounds, while the second step takes place above 230 °C. The exception is again the malonic acid derived **2-l**, which decomposes at significantly lower temperatures. This two-step decomposition is consistent with the structural composition of these TBGs containing two equivalent carboxylate groups, each associated with one TBD counterion. The observation of two separate decomposition events suggests that the initial base release from one anionic site does not trigger immediate cleavage of the second. Instead, the system appears to reach a temporarily stabilized intermediate state before the second activation occurs. No clear trend is evident for the first activation temperature ($T_{TBG\text{-}ACT\text{-}1}$), which lies within a narrow range between 63 °C and 76 °C for all compounds. In contrast, the second activation temperature ($T_{TBG\text{-}ACT\text{-}2}$) reveals a notable structure–property relationship. As with the partially neutralized analogues, the thermal stability at this stage increases with the chain length, following the order: **2-n** > **2-m** > **2-k** > **2-l** (Fig. 3d and e). This indicates that, with the exception of **2-l**, an increased number of $-CH_2$-moieties between carboxylate groups enhances thermal stability.[60] A notable phenomenon observed is the lack of immediate mass loss following the first activation event, even when the temperature exceeds the known thermal threshold of free TBD (~200 °C). In its pure form, TBD exhibits rapid evaporation and decomposition above this temperature as confirmed by TGA (see SI Fig. S13). However, in the solid TBG, the system remains thermally stable up to significantly higher temperatures, often beyond 250 °C, before a second, more pronounced weight loss step is observed. This pattern strongly suggests that the initial thermally triggered cleavage of the salt linkage, expected to release one of the two TBD units, does not result in full liberation of the free, volatile base. Instead, the data supports the formation of a thermally stabilized intermediate, in which the base remains sequestered in the solid matrix. One possible mechanism might be the formation of ion pair or zwitterionic intermediates with the remaining carboxylate.[61] This interaction reduces volatility and prevent premature desorption of TBD from the matrix. Another explanation might be residual proton donors or neighboring polar groups that form hydrogen bonds with the released TBD, further impeding its escape from the matrix until higher thermal energy is applied.[62] An exception to this behavior is again clearly observed with **2-l**, derived from malonic acid. Instead of exhibiting delayed mass loss, **2-l** undergoes rapid decomposition above ~200 °C, coinciding precisely with the expected volatilization of pure TBD. In contrast to its homologues, no intermediate stabilization is evident. Upon heating, a fast cleavage occurs, likely through a concerted decarboxylation or fragmentation pathway, liberating TBD without the formation of a stabilizing intermediate. Moreover, due to the limited number of $-CH_2-$ units, steric confinement of TBD is less effective, making free diffusion and evaporation of TBD more favorable.[63] As a result, **2-l** shows early and efficient base release.

To better understand the effect of structural modification on the thermal release behavior of TBGs, the activation temperatures of partly neutralized TBGs (**2-f** and **2-h–j**) were compared with their fully neutralized analogues (**2-k–n**). These pairs are based on the same dicarboxylic acid backbone but differ in the number of coordinated TBD equivalents—either one (partial neutralization) or two (full neutralization). For **2-k** (oxalate) and **2-m** (succinate), full neutralization increases the activation temperature, likely due to stronger electrostatic stabilization and reduced reactivity of the intermediate.[64] The increase in chain length (C2 → C4) appears to enhance thermal resilience when both acid groups are blocked. **2-l** (malonate) cleaves earlier than **2-h**, likely due to intrinsic decarboxylation tendencies of the malonate structure (β-keto acid analogue), leading to early fragmentation irrespective of the degree of neutralization.[58] **2-n** (adipate) surprisingly activates earlier than **2-j**, despite having both groups neutralized. A plausible

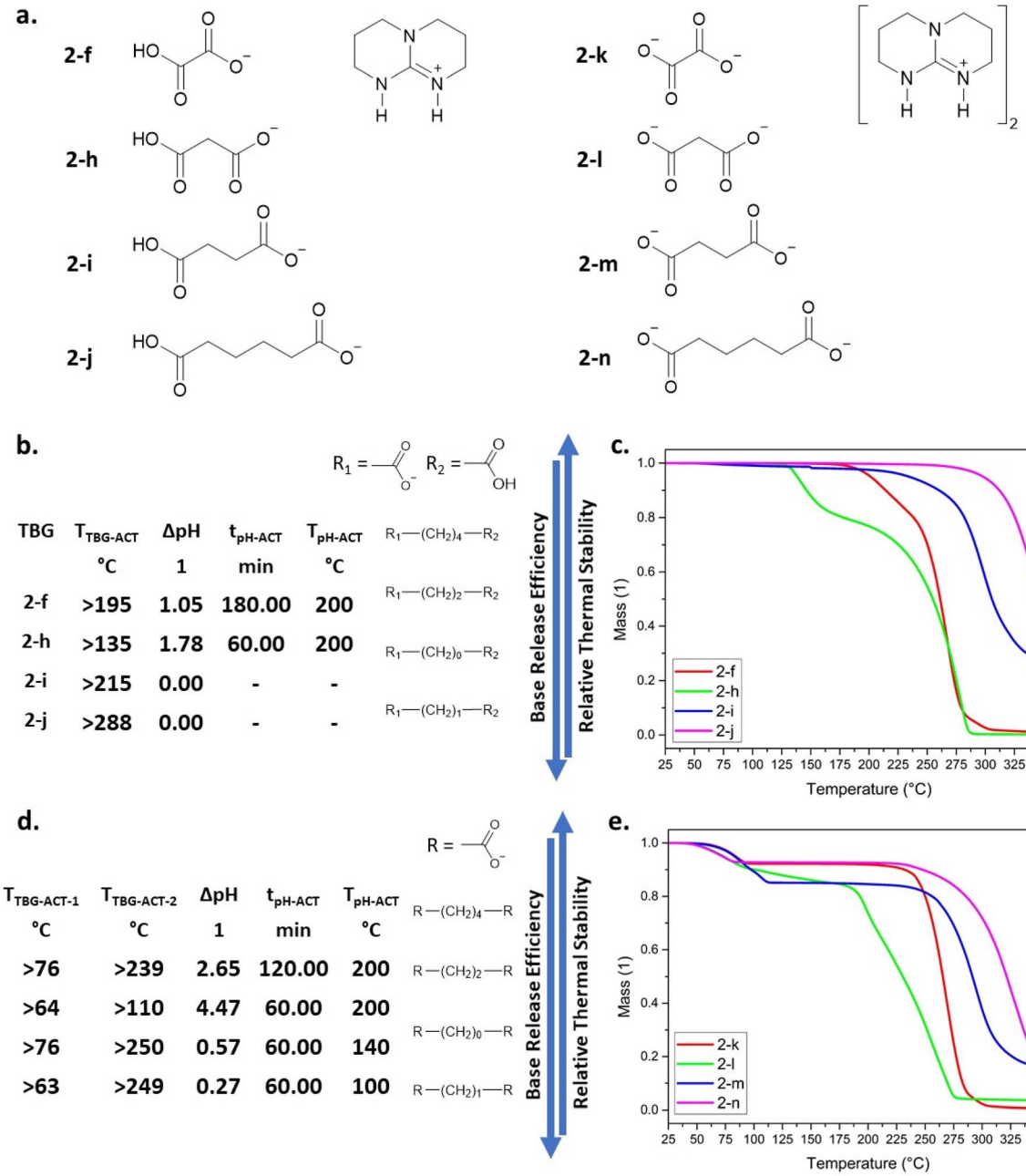

Fig. 3 Influence of stabilization groups varying in spacer length and degree of neutralization on the properties of TBD releasing QASs. (a) Chemical structures of the synthesized TBGs **2-f** and **2-h–n**. (b and d) Summary of $T_{TBG-ACT}$, ΔpH after activation, t_{pH-ACT}, and T_{pH-ACT}; including a schematic representation of the relative thermal stability, base release efficiency, and initial activation of the carboxylic acids. TGA analysis of the TBGs (c) **2-f** and **2-h–j** and (e) **2-h–n**.

explanation lies in long-chain flexibility, which may facilitate internal diffusion and release of one TBD even before the second activation, effectively lowering $T_{TBG-ACT2}$.[65] This proposed two-step release mechanism is supported by later pH-measurements, which indicate base release during the first thermal event observed in the TGA (see SI, Table S24). In some fully neutralized TBGs (*e.g.*, **2-k**, **2-m**), the second activation temperature is higher than in their partly neutralized counterparts, which indicates that the first cleavage step forms a stable intermediate, potentially stabilized by internal hydrogen bonding or charge delocalization. Conversely, where $T_{TBG-ACT2} < T_{TBG-ACT}$ (*e.g.*, **2-l**, **2-n**), the second cleavage may be structurally favored or entropically driven, especially when chain flexibility or unstable intermediates (such as malonate) are involved.[66]

EGA-FTIR was employed to investigate the thermal activation behavior of compounds **2-f** and **2-h–2-m** (Fig. S35–S48). The partly neutralized TBGs (**2-f**, **2-h**, and **2-i**) all exhibited an initial, clean release of CO_2, followed, upon further heating, by a simultaneous release of CO_2, base (TBD), and other side products. In contrast, the fully neutralized derivatives (**2-k**, **2-l**,

and **2-m**) did not show this early CO_2 release, but with otherwise comparable spectral features to their partly neutralized counterparts. These observations support the conclusion that the initial CO_2 release in partly neutralized TBGs arises from free (unblocked) carboxylate groups.[67] After this first decarboxylation step, the cleavage behavior of the partly neutralized compounds mirrors that of the fully neutralized analogues. An exception to this trend is observed in the adipic acid-based TBGs (**2-j** and **2-n**). Both compounds show identical gas evolution profiles, with no early CO_2 release in the partly neutralized compound **2-j**. Instead, both begin releasing CO_2 and base simultaneously starting at around 280 °C, suggesting a distinct cleavage mechanism independent of neutralization degree. For the oxalate-based derivatives, the partly neutralized **2-f** shows an initial CO_2 release between 180–220 °C. Subsequently, both **2-f** and its fully neutralized analogue **2-k** begin releasing CO_2 and TBD simultaneously at 240 °C. Notably, no side products are detected, and only the characteristic peaks of CO_2 and TBD are observed. These results strongly suggest a clean decarboxylation mechanism, without evidence of condensation or secondary side reactions. The malonate derivatives show subtler differences. Compound **2-h** exhibits initial CO_2 release between 120–160 °C. From 180 °C onward, no further CO_2 is observed, but strong signals corresponding to TBD evolution appear. Additionally, starting at 200 °C, new peaks arise at 3400–3000, 1800–1750 cm^{-1} and 1175 cm^{-1}, consistent with dehydration upon anhydride formation.[49] For **2-l**, cleavage begins between 140–160 °C with CO_2 evolution. At 180 °C, a simultaneous release of CO_2 and TBD is observed, followed by exclusive base evolution and the emergence of the same anhydride-associated IR peaks from 200 °C onward. These observations support the following cleavage mechanism for **2-h** and **2-l**: the first step is thermal decarboxylation, favored due to the intrinsic reactivity of malonate derivatives (beta-keto acid).[58] In **2-h**, this results in CO_2 release alone; in **2-l**, both CO_2 and TBD are released. The remaining acetate species (bound to TBD) subsequently undergo cleavage *via* anhydride formation, analogous to previously studied compound **2-a**, with closely matching thermal profiles. In the succinate-based systems, **2-i** (partly neutralized) shows an initial CO_2 release between 200–220 °C, followed by simultaneous evolution of CO_2 and TBD between 240–280 °C, without detectable side products. At 300 °C, new peaks again appear between 3400-3000, 1800–1750 cm^{-1} and at 1175 cm^{-1}, indicating secondary anhydride formation. The fully neutralized **2-m** follows the same behavior, except without the early CO_2 release. Thus, both compounds likely undergo decarboxylation upon base release, followed by side reactions at higher temperatures. Finally, both **2-j** and **2-n** (adipate-based) are thermally stable up to 280 °C, after which a sharp release of CO_2 and TBD is observed. Interestingly, several lower-frequency TBD peaks (1490–1440 and 1360–1325 cm^{-1}) are either missing or strongly overlapped. Instead, new bands appear at 3400–3000, 1575–1525, 1425, 1375, and 1310 cm^{-1}, which can be attributed to anhydride formation[49] (linear or cyclic) or ketonization[16] reactions. These spectral features suggest that the cleavage mechanism involves CO_2 release followed by either anhydride formation or ketonization.

Subsequently, the temperature-dependent ΔpH of selected compounds was measured in DMSO/water mixtures (see SI Tables S18–S24). Compounds **2-h**, **2-k**, and **2-l** exhibit a pH activation profile similar to that of **2-f**, as discussed in the prior chapter. Each shows the most pronounced ΔpH at its respective $t_{pH\text{-}ACT}$ and $T_{pH\text{-}ACT}$ values. For **2-h** and **2-l** initial ΔpH are already observed starting at temperatures as low as 120 °C. Notably, these activation profiles in solution align well with their $T_{TBG\text{-}ACT}$ values observed in the solid state. However, prolonged heating at 200 °C results in a noticeable decline in basicity, indicating the onset of secondary reactions. A comparison of partially *versus* fully neutralized analogues, **2-f** *vs.* **2-k** and **2-h** *vs.* **2-l**, reveals that full neutralization leads to a significantly greater base release. While a twofold increase in ΔpH is expected based on stoichiometry, the observed ΔpH values exceed this, suggesting that fully neutralized compounds undergo a more complete and cleaner activation. In contrast, partially neutralized species may undergo side reactions that reduce the effective basicity and consume portions of the released base. Compounds **2-i** and **2-j** showed no measurable pH increase, consistent with their high $T_{TBG\text{-}ACT}$ values (215 °C and 288 °C, respectively). These results suggest that under the experimental conditions, these derivatives are thermally too stable to undergo significant base release. Their increased stability is likely due to longer aliphatic chains or steric hindrance, which inhibit decarboxylation. Moreover, at the required activation temperatures, side reactions are more likely to occur than selective base release. Interestingly, compounds **2-m** and **2-n** displayed a unique biphasic activation profile not observed in other derivatives. Upon heating to relatively low temperatures, 140 °C for **2-m** and 100 °C for **2-n**, a modest but distinct pH increase was observed (ΔpH = 0.57 and 0.27, respectively), corresponding to an initial activation step ($T_{TBG\text{-}ACT1}$). After this first shift, the pH plateaued or even declined, with no further increase observed, indicating that full base release was not achieved. TGA data strongly support this two-step activation mechanism. This behavior correlates with the carbon spacer length of the anionic moiety: **2-n**, with the longest spacer, begins to cleave at the lowest temperature (100 °C), followed by **2-m** at 140 °C. In contrast, **2-l** also activates at 140 °C but undergoes full cleavage, while **2-k**, with the shortest chain, requires 200 °C for complete activation. This trend suggests that in solution, longer spacer lengths reduce the thermal threshold for the initial cleavage ($T_{TBG\text{-}ACT1}$), while shorter chains increase it. For **2-m** and **2-n**, the temperature gap between $T_{TBG\text{-}ACT1}$ and $T_{TBG\text{-}ACT2}$ is sufficiently large to allow the formation of stable intermediates, effectively halting full activation under the given thermal conditions. In contrast, for **2-l** and **2-k**, these two steps overlap, preventing intermediate stabilization and leading to rapid, complete decarboxylation in a single thermal event. The high ΔpH values observed for **2-l** and **2-k** further confirm this clean and efficient release. As discussed in previous chapters, these findings underscore the differing behaviors of TBGs in solid *versus* solution states. Importantly, they highlight a key consideration for future applications: TGA-derived activation temperatures may not directly translate to performance in real systems, particularly when TBGs are dissolved in polymeric

matrices. Interactions with the matrix can either stabilize or destabilize the active species. Therefore, careful assessment of the activation environment is essential for designing and predicting the performance of TBGs in functional materials.

To investigate how the degree of neutralization affects the thermal activation behavior of TBGs a multivariate correlation analysis was conducted using $T_{TBG\text{-}ACT}$ as the main descriptor of interest. A set of independent variables was chosen to capture both electronic and structural properties: pK_{a1} and pK_{a2} values from literature,[53] $pH_{NOT\text{-}ACT}$ and ΔpH. In addition, three semi-quantitative structural descriptors were ranked to enable correlation: decarboxylation behavior (1 = no decarboxylation; 5 = clean decarboxylation with base release, based on EGA data), carbon spacer length (number of carbon atoms between the two carboxylic groups), and the neutralization degree (1 = partially neutralized, 2 = fully neutralized). A low-temperature mass loss event observed in the fully neutralized samples ($T_{TBG\text{-}ACT1}$) was interpreted as physical water desorption, not chemical cleavage, and therefore excluded from the analysis. Only $T_{TBG\text{-}ACT2}$ (with observed base release, based on EGA data) was used for correlation. The full Pearson correlation matrix is provided in the SI (Table S31), allowing assessment of interdependencies between all variables. The input parameters are shown in Table S30.

Notably, pK_{a1} showed a strong negative correlation with $T_{TBG\text{-}ACT2}$ ($r = -1.00$), suggesting that higher acidic dicarboxylic acids form salts that require higher thermal energy to dissociate in the first degradation step. In contrast, pK_{a2} was positively correlated ($r = +1.00$), reflecting that the second deprotonation step plays an opposite role in stabilizing the fully neutralized species. Likewise, $pH_{NOT\text{-}ACT}$ correlated strongly and positively ($r = +0.99$), confirming that less acidic salts in the pre-activated state are easier to activate thermally. ΔpH showed a strong negative correlation ($r = -0.94$), indicating that systems capable of large pH changes tend to require lower $T_{TBG\text{-}ACT}$.

Decarboxylation behavior, as expected, exhibited a perfect negative correlation ($r = -1.00$) with $T_{TBG\text{-}ACT}$, confirming that systems with clean CO_2 release undergo activation at lower temperatures. Spacer length, correlated positively ($r = +1.00$), highlighting that longer, more flexible acids lead to more thermally stable salts. Finally, the neutralization parameter was strongly negatively correlated ($r = -0.97$), meaning that fully neutralized systems dissociate at higher temperatures, likely due to the absence of free acidic protons that might promote cleavage or destabilize the salt.

Taken together, these results underscore how electronic acidity (pK_{a1}/pK_{a2}), structural flexibility (spacer length), and the degree of neutralization cooperate to govern thermal decomposition. Moreover, the strong correlations validate the approach of combining experimental values with semi-quantitative descriptors in predictive analysis and point to decarboxylation efficiency and salt topology as key design parameters for tunable TBGs.

3 Conclusions

A comprehensive library of TBGs with tunable cleavage temperatures ranging from 60 °C to 290 °C was successfully synthesized and characterized for potential application in dynamic polymer networks. TGA enabled the determination of $T_{TBG\text{-}ACT}$ across all compounds in the solid state, with initial decarboxylation steps contributing to the mass loss. EGA-FTIR provided mechanistic insights into the cleavage pathways and confirmed the release of the base. pH-measurements in solution further demonstrated activation upon base release, consistent with the TGA and EGA-FTIR results. Systematic variation of either the cationic base or the anionic leaving group revealed that the cleavage temperature was significantly influenced by the nature of the base, while the cleavage mechanism remained consistent across different bases with a common cyanoacetate anion (**1-a–e**). All TBGs underwent clean decarboxylation, as expected from cyanoacetic acid derivatives. Two distinct trends were observed among guanidine-based TBGs: (1) higher basicity generally correlated with increased thermal stability, and (2) bases with higher nucleophilicity, despite lower basicity, also showed enhanced thermal stability. Additionally, a correlation between the nucleophilicity of base (**1-c** and **1-f**) and pH value in the not-activated state of the TBG was found. These findings suggest that nucleophilicity has a more pronounced impact on thermal stability than basicity alone when designing TBG systems. Bases with boiling/degradation temperatures close to the $T_{TBG\text{-}ACT}$ (*e.g.*, **1-d**, **1-f**) exhibited a single-step mass loss, while thermally stable bases, with boiling/degradation far above $T_{TBG\text{-}ACT}$ (*e.g.*, **1-a**, **1-b**, **1-c**, **1-e**) showed a two-step process: initial base release followed by subsequent evaporation at elevated temperatures. Further investigations focused on TBGs containing the same basic building block (TBD) and selected acetic and dicarboxylic acid derivatives as anions. For acetate mono substituted acetic acid derivatives-based TBGs, clear structure–stability relationships were identified. Electron-withdrawing substituents did not inherently lower thermal stability; rather, stability was governed by the ability to form stabilized carbanions. For example, TBGs bearing cyano groups (**1-a**) or trichloro substituents (**2-d**) demonstrated clean release and full base liberation, confirmed *via* pH-measurements and EGA-FTIR. In contrast, high $T_{TBG\text{-}ACT}$ led to undesired side reactions and decomposition, as evidenced by a slight shift of the pH value (or even a shift to lower more acidic pH values). The comparison of partially *versus* fully neutralized dicarboxylic acid-based TBGs revealed that partially neutralized compounds (*e.g.*, **2-f**, **2-h** to **2-j**) showed increasing thermal stability with longer aliphatic chains, particularly when β-keto structures were absent. Fully neutralized TBGs displayed two distinct activation events, not always visible in TGA (solid state) but detectable in solution *via* pH-measurements and EGA-FTIR analysis. Short-chain mono substituted acetic acid derivatives (**2-k**, **2-l**) exhibited overlapping activation steps, resulting in a single cleavage event and complete base release. In contrast, longer-chain analogues (**2-m**, **2-n**) showed an initial activation event followed by thermal stabilization, with only the first cleavage step occurring and no further decomposition. Additionally, it was observable that the medium in which the TBGs were activated (DMSO/water) has a high influence on the thermal stability of the TBGs and can reduce the thermal stability significantly compared with the undissolved solid-state

counterparts (*e.g.* **1-a** and **2-e**). Finally, during this study decarboxylation, condensation, dehydration and ketonization have been observed as cleavage mechanisms for selective base release. These findings provide a robust framework for the design of TBGs with predictable thermal behavior. In follow-up studies, the synthesized TBGs will be incorporated into dynamic polymer networks to evaluate their performance as thermally switchable catalysts. In follow-up studies, the synthesized TBGs will be incorporated into dynamic polymer networks to evaluate their performance as thermally latent catalysts. Beyond their technical performance, the integration of TBGs into dynamic polymer networks systems offers notable sustainability benefits. The ability to reshape and reuse polymeric materials without loss of performance directly supports circular material strategies by extending service lifetimes, minimizing waste generation, and reducing reliance on energy- and resource-intensive virgin production. By enabling controlled reprocessing, TBG-based vitrimers can help lower energy consumption, decrease greenhouse gas emissions, and contribute to carbon neutrality objectives within the polymer industry.

Conflicts of interest

There are no conflicts to declare.

Data availability

The data supporting this article have been included as part of the SI.

Supplementary information: Experimental part, NMR, FTIR-spectra, DSC, DTG-curve and EGA-FTIR analysis of thermolatent bases. See DOI: **https://doi.org/10.1039/d5ra05095b**.

Acknowledgements

The research work was carried out within the COMET-Module project "Repairtecture" (project-no.: 904927) at the Polymer Competence Center Leoben GmbH (PCCL, Austria) within the framework of the COMET-program of the Federal Ministry for Innovation, Mobility and Infrastructure and the Federal Ministry of Economy, Energy and Tourism. The COMET-Module is funded by the Austrian Government and the State Governments of Styria and Upper Austria. Part of the research was also conducted within the production of the future project "CircularEpoxy" (project number: 58728995), which received funding from the Austrian Research Promotion Agency (FFG). Funding was also provided by the OEAD project "Multi-material 3D printing with functional methyl methacrylate resins" between Croatia and Austria (project number: HR02/2024).

References

1 (*a*) Y. Yağci and I. Reetz, *Prog. Polym. Sci.*, 1998, **23**, 1485–1538; (*b*) Y. Yang, F.-S. Du and Z.-C. Li, *ACS Appl. Polym. Mater.*, 2020, **2**, 5630–5640.

2 T. Vidil, F. Tournilhac, S. Musso, A. Robisson and L. Leibler, *Prog. Polym. Sci.*, 2016, **62**, 126–179.

3 (*a*) J. Deng, S. Bailey, S. Jiang and C. K. Ober, *Chem. Mater.*, 2022, **34**, 6170–6181; (*b*) N. Zivic, P. K. Kuroishi, F. Dumur, D. Gigmes, A. P. Dove and H. Sardon, *Angew. Chem., Int. Ed.*, 2019, **58**, 10410–10422; (*c*) L. Song, Q. Ye, X. Ge, A. Misra and P. Spencer, *Acta Biomater.*, 2016, **35**, 138–152.

4 J. V. Crivello, *Cationic Polymerization — Iodonium and Sulfonium Salt Photoinitiators*, Springer-Verlag, 2005.

5 C. J. Martin, G. Rapenne, T. Nakashima and T. Kawai, *J. Photochem. Photobiol., C*, 2018, **34**, 41–51.

6 K. SUYAMA and M. SHIRAI, *Prog. Polym. Sci.*, 2009, **34**, 194–209.

7 (*a*) A. Romano, I. Roppolo, M. Giebler, K. Dietliker, Š. Možina, P. Šket, I. Mühlbacher, S. Schlögl and M. Sangermano, *RSC Adv.*, 2018, **8**, 41904–41914; (*b*) J. Sinha, S. Soars and C. N. Bowman, *Macromolecules*, 2021, **54**, 1693–1701; (*c*) K. Dietliker, R. Hüsler, J.-L. Birbaum, S. Ilg, S. Villeneuve, K. Studer, T. Jung, J. Benkhoff, H. Kura, A. Matsumoto and H. Oka, *Prog. Org. Coat.*, 2007, **58**, 146–157.

8 F. Ricciardi, W. A. Romanchick and M. M. Joullié, *J. Polym. Sci., Part B*, 1983, **21**, 633–638.

9 (*a*) M. Kim, F. Sanda and T. Endo, *Macromolecules*, 2000, **33**, 3499–3501; (*b*) M. Kim, F. Sanda and T. Endo, *Macromolecules*, 2001, **34**, 409–414.

10 M. Kirino and I. Tomita, *Macromolecules*, 2010, **43**, 8821–8827.

11 (*a*) I. Bianchi, L. Greco, C. Mignanelli, M. Simoncini and A. Vita, *Procedia CIRP*, 2024, **122**, 1059–1064; (*b*) A. Mariani and G. Malucelli, *Chem. Commun.*, 2025, **61**, 2173–2189.

12 D. Reisinger, M. U. Kriehuber, M. Bender, D. Anguis-Bautista, B. Rieger and S. Schlögl, *Adv. Mater.*, 2023, **35**(24), e2300830.

13 D. Reisinger, A. Sietmann, A. Das, S. Plutzar, R. Korotkov, E. Rossegger, M. Walluch, S. Holler-Stangl, T. S. Hofer, F. Dielmann, F. Glorius and S. Schlögl, *Adv. Mater.*, 2024, **36**, 2411307.

14 S. Tshepelevitsh, A. Kütt, M. Lõkov, I. Kaljurand, J. Saame, A. Heering, P. G. Plieger, R. Vianello and I. Leito, *Eur. J. Chem.*, 2019, **40**, 6735–6748.

15 S. O. C. Mundle, G. Lacrampe-Couloume, B. Sherwood-Lollar and R. Kluger, *J. Am. Chem. Soc.*, 2010, **132**(7), 2430–2436.

16 (*a*) S. C. Moldoveanu, *Techniques and Instrumentation in Analytical Chemistry*, 2010, vol. 28, pp. 471–526; (*b*) M. Renz, *Eur. J. Chem.*, 2005, **6**, 979–988.

17 L. F. Fieser, E. L. Martin and R. L. Shriner, *Org. Synth.*, 1932, **12**, 66.

18 (*a*) E. Schuler, L. Grooten, M. Kasireddy, S. More, S. N. Raveendran, S. Tanielyan, R. L. Augustine and G. J. M. Gruter, *Green Chem.*, 2023, **25**, 2409–2426; (*b*) T. Winkler, F. Baccot, K. Eränen, J. Wärna, G. Hilpmann, R. Lange, M. Peurla, I. Simakova, H. Grénman, D. Y. Murzin and T. Salmi, *Catal. Today*, 2022, **387**, 128–139.

19 E. C. Griffith, B. K. Carpenter, R. K. Shoemaker and V. Vaida, *Proc. Natl. Acad. Sci. U. S. A.*, 2013, **110**(29), 11714–11719.

20 (*a*) Z. Zong, Q. Zhang and D.-H. Qu, *Chem.–Eur. J.*, 2022, **28**(68), e202202462; (*b*) D. P. Valencia, P. D. Astudillo,

A. Galano and F. J. Gonzáles, *Org. Biomol. Chem.*, 2013, **11**, 318–325.
21 L. W. Clark, *Int. J. Chem. Kinet.*, 1974, **6**(5), 713–724.
22 M. Baidya and H. Mayr, *Chem. Commun.*, 2008, **15**, 1792–1794.
23 (*a*) Y. Cai, A. M. Chippindale, R. J. Curry and P. Vaqueiro, *Inorg. Chem.*, 2021, **60**(7), 5333–5342; (*b*) D. A. Dougherty, *Chem. Rev.*, 2025, **125**(5), 2793–2808.
24 S. Datta and T. Limpanuparb, *RSC Adv.*, 2021, **11**, 20691–20700.
25 (*a*) B. Zhang, S. D. Zarić, S. S. Zrilić, I. Gofman, B. Heck and G. Reiter, *Commun. Chem.*, 2025, **8**, 21; (*b*) K. Carter-Fenk and J. M. Herbert, *Chem. Sci.*, 2020, **11**, 6758–6765; (*c*) B. Schramm, M. Gray and J. Herbert, *ChemRxiv*, 2024, preprint, DOI: 10.26434/chemrxiv-2024-5k2b8-v2.
26 F. Carrillo-Hermosilla, R. Fernández-Galán, A. Ramos and D. Elorriaga, *Molecules*, 2022, **27**(18), 5962.
27 (*a*) V. P. Sharma, V. Kumar, P. Sonker, P. Yadav, R. Singh, R. Gnanasekaran and A. K. Tewari, *Eur. J. Org Chem.*, 2023, **26**(48), e202301109; (*b*) J. Xu, *Molecules*, 2024, **29**(7), 1454; (*c*) C. A. Hunter and J. K. M. Sanders, *J. Am. Chem. Soc.*, 1990, **112**, 5525–5534.
28 D. Reisinger, A. Hellmayr, M. Paris, M. Haas, T. Griesser and S. Schlögl, *Polym. Chem.*, 2023, **14**, 3082.
29 E.-M. Köck, M. Kogler, T. Bielz, B. Klötzer and S. Penner, *J. Phys. Chem.*, 2013, **117**(34), 17666–17673.
30 N. Chakrabortya and A. K. Mitra, *Org. Biomol. Chem.*, 2023, **21**, 6830–6880.
31 R. Nicholls, S. Kaufholda and B. N. Nguyen, *Catal. Sci. Technol.*, 2014, **4**, 3458–3462.
32 T. H. Nguyen, D. E. Hibbs and S. T. Howard, *J. Comput. Chem.*, 2005, **26**(12), 1233–1241.
33 E. C. Johnson, K. P. Gregory, H. Robertson, I. J. Gresham, A. R. J. Nelson, V. S. J. Craig, S. W. Prescott, A. J. Page, G. B. Webber and E. J. Wanless, *Chem. Sci.*, 2025, **16**, 2382–2390.
34 L. R. Domingo, J. Andrés, V. Moliner and V. S. Safont, *J. Am. Chem. Soc.*, 1997, **119**(27), 6415–6422.
35 M. M. De Villiers, D. E. Wurster and K. Narsai, *J. Soc. Cosmet. Chem.*, 1997, **48**(4), 165–174.
36 A. L. C. S. do Nascimento, J. A. Teixeira, W. D. G. Nunes, D. J. C. Gomes, C. Gaglieri, O. Treu-Filho, M. Pivatto, F. J. Caires and M. Ionashiro, *J. Therm. Anal. Calorim.*, 2017, **130**, 1463–1472.
37 J. Krupa, I. Kosendiak, M. Wierzejewska and J. Lundell, *Spectrochim. Acta, Part A*, 2025, **325**, 125081.
38 J. Clayden, N. Greeves, S. Warren and P. Wothers, *Organic Chemistry*, Oxford University Press, Oxford, 2001.
39 R. A. L. Peerboom, L. J. de Koning and N. M. M. Nibbering, *J. Am. Soc. Mass Spectrom.*, 1994, **5**, 159–168.
40 D. A. Dixon, P. A. Charlier and P. G. Gassman, *J. Am. Chem. Soc.*, 1980, **102**(11), 3957–3959.
41 P. J. Atkins, V. Gold and R. Marsh, *J. Chem. Soc., Perkin Trans. 2*, 1984, (7), 1239–1245.
42 G. C. Q. da Silva, T. M. Cardozo, G. W. Amarante, C. R. A. Abreu and B. A. C. Horta, *Phys. Chem. Chem. Phys.*, 2018, **20**(34), 21988–21998.
43 M. Ziegler-Borowska, D. Chełminiak, H. Kaczmarek and A. Kaczmarek-Kędziera, *J. Therm. Anal. Calorim.*, 2016, **124**(3), 1267–1280.
44 X.-J. Wang and J.-Z. You, *J. Therm. Anal. Calorim.*, 2015, **120**(3), 1009–1025.
45 H. Neuvonen, K. Neuvonen, A. Koch, E. Kleinpeter and P. Pasanen, *J. Org. Chem.*, 2002, **67**(20), 6995–7003.
46 M. C. Elliott, C. E. Hughes, P. J. Knowles and B. D. Ward, *Org. Biomol. Chem.*, 2025, **23**, 352–359.
47 C. Tang, J. Peng, X. Li, Z. Zhai, H. Gao, W. Bai, N. Jiang and Y. Liao, *Korean J. Chem. Eng.*, 2016, **33**, 99–106.
48 (*a*) A. Varenikov, E. Shapiro and M. Gandelman, *Chem. Rev.*, 2021, **121**(1), 412–484; (*b*) M. B. Gawande, S. S. Deshpande, J. R. Satam and R. V. Jayaram, *Catal. Commun.*, 2007, **8**(3), 576–582.
49 X. Gu and C. Q. Yang, *Res. Chem. Intermed.*, 1998, **24**, 979–996.
50 (*a*) M. Friedman and H. S. Jürgens, *J. Agric. Food Chem.*, 2000, **48**(6), 2101–2110; (*b*) J. A. Manion, D. F. McMillen and R. Malhotra, *Energy Fuels*, 1996, **10**, 776–788.
51 (*a*) E. Gazagnaire, J. Helminen, T. Golin Almeida, P. Heinonen, M. Metsälä, T. Kurten and I. Kilpeläinen, *RSC Adv.*, 2025, **15**, 4945–4951; (*b*) J. Witos, K. Ojha, P. Uusi-Kyyny, V. Alopaeus, I. Kilpeläinen, H. Sixta and I. Schlapp-Hackl, *Ind. Eng. Chem. Res.*, 2022, **61**, 259–268.
52 J. B. Washington, M. Assante, C. Yan, D. McKinney, V. Juba, A. G. Leach, S. E. Baillied and M. Reid, *Chem. Sci.*, 2021, **12**, 6949–6963.
53 (*a*) E. A. Braude and F. C. Nachod, *Determination of Organic Structures by Physical Methods*, Academic Press, New York, 1955; (*b*) R. M. C. Dawson, D. C. Elliott, W. H. Elliott and K. M. Jones, *Data for Biochemical Research*., Oxford University Press, London, 1959; (*c*) J. F. J. Dippy, S. R. C. Hughes and A. Rozanski, *J. Chem. Soc.*, 1959, 2492–2498.
54 (*a*) M. E. Brown, *Introduction to Thermal Analysis: Techniques and Applications*, Springer, Dordrecht, 2nd edn, 2001; (*b*) H. E. Kissinger, Variation of peak temperature with heating rate in differential thermal analysis, *J. Res. Natl. Bur. Stand.*, 1956, **57**, 217–221.
55 (*a*) J. M. J. Swanson, C. M. Maupin, H. Chen, M. K. Petersen, J. Xu, Y. Wu and G. A. Voth, *J. Phys. Chem. B*, 2007, **111**(17), 4300–4314; (*b*) B. Antalicz and H. J. Bakker, *JACS Au.*, 2024, **4**(8), 2995–3006.
56 S. Shen and A. A. Skordos, *Eur. Polym. J.*, 2025, **228**, 113812, DOI: 10.1016/j.eurpolymj.2025.113812.
57 K. Pahnke, J. Brandt, G. Gryn'ova, P. Lindner, R. Schweins, F. G. Schmidt, A. Lederer, M. L. Coote and C. Barner-Kowollik, *Chem. Sci.*, 2015, **6**, 1061–1074.
58 (*a*) P. G. Maiella and T. B. Brill, *J. Phys. Chem.*, 1996, **100**(34), 14352–14355; (*b*) A. V. Ignatchenko, M. E. Springer, J. D. Walker and W. W. Brennessel, *J. Phys. Chem.*, 2021, **125**(6), 3368–3384.
59 H. T. Chen, J. G. Chang, D. G. Musaev and M. C. Lin, *J. Phys. Chem.*, 2008, **112**(29), 6621–6629.
60 (*a*) T. H. Nguyen, D. E. Hibbs and S. T. Howard, *J. Comput. Chem.*, 2005, **26**(12), 1233–1241; (*b*) J. Zotova, B. Twarnley

and L. Tajber, *Mol. Pharmaceutics*, 2022, **19**(8), 2980–2991; (*c*) L. Al-Seakh, S. Fritsch, A. Appelhagen, A. Villinger and R. Ludwig, *Molecules*, 2022, **27**(2), 366.

61 I. Negi, R. Jangra, A. Gharu, J. F. Trant and P. Sharma, *Phys. Chem. Chem. Phys.*, 2023, **25**, 857–869.

62 (*a*) J. N. Scott, N. V. Nucci and J. M. Vanderkooi, *J. Phys. Chem. A*, 2008, **112**(43), 10939–10948; (*b*) D. Rauber, F. Philippi, J. Becker, J. Zapp, B. Morgenstern, B. Kuttich, T. Kraus, R. Hempelmann, P. Hunt, T. Welton and C. W. M. Kay, *Phys. Chem. Chem. Phys.*, 2023, **25**, 6436–6453.

63 (*a*) V. L. Stanford and S. Vyazovkin, *Ind. Eng. Chem. Res.*, 2017, **56**(28), 7964–7970; (*b*) C. L. Perrin, A. Flach and M. N. Manalo, *J. Am. Chem. Soc.*, 2012, **134**(23), 9698–9707.

64 (*a*) R. N. Khlestkin, V. L. Khlestkina, R. B. Valitov and N. G. Usanov, *React. Kinet. Catal. Lett.*, 1981, **17**, 391–392; (*b*) F. J. Caires, L. S. Lima, C. T. Carvalho and M. Ionashiro, *Thermochim. Acta*, 2010, **500**(1–2), 6–12, DOI: **10.1016/j.tca.2009.11.015**.

65 W. Sun, P. Pinacho, D. A. Obenchain and M. Schnell, *J. Phys. Chem. Lett.*, 2024, **15**(3), 817–825.

66 G. Gilli and P. Gilli, *The Nature of the Hydrogen Bond: Outline of a Comprehensive Hydrogen Bond Theory*, Oxford University Press, Oxford, 2009.

67 L. J. Adams, B. Franzus and T. T.-S. Huang, *Int. J. Chem. Kinet.*, 1978, **10**(7), 669–675.